Development of capsaicin derivatives as prohibitin ligands to modulate the Aurora kinase A/PHB2 interaction in cancer cells

Amel Djehal[a,b,‡], Claire Caron[c,‡], Valentina Pizza[c], Kimberley Farin[b], Giulia Bertolin[c,*] and Laurent Désaubry[b,*]

[a]Higher National School of Biotechnology of Constantine, Constantine 25100, Algeria

[b]Laboratory of Regenerative Nanomedicine, Center of Research and Biomedicine, University of Strasbourg, 67000 Strasbourg, France

[c]CNRS, Univ Rennes, IGDR [(Institut de Génétique et Développement de Rennes)] - UMR 6290, F-35000 Rennes, France

‡ Contributed equally to this work

*To whom correspondence should be addressed: giulia.bertolin@univ-rennes.fr (G.B), desaubry@unistra.fr (L.D.)

Keywords: PHB2; Aurora kinase A/AURKA; capsaicin; mitochondria; FRET/FLIM microscopy, cancer.

Abstract

Aurora kinase A/AURKA is a serine/threonine kinase overexpressed in a variety of solid and hematological malignancies. In the last decades, clinical trials aiming to counteract the overexpression of AURKA turned out to be largely unsuccessful. Meanwhile, recent discoveries pointed at new functions of AURKA at the subcellular level, including at mitochondria. At this location, AURKA induces organelle clearance by mitophagy by acting in complex with the mitophagy mediator LC3, and its inner mitochondrial membrane receptor PHB2. The natural polyphenol xanthohumol was shown to act as a PHB2 ligand, altering the interaction between AURKA and PHB2 and restoring mitochondrial functions in cancer cells. However, its chemical nature prevents its broader use as an anti-cancer agent.

Using Förster's Resonance Energy Trasfer/Fluorescence Lifetime Imaging Microscopy (FRET/FLIM) in live breast cancer cells, we here explore the effects of alternative PHB ligands in altering the proximity between AURKA and PHB2. Among the already-available compounds, we found that the pungent natural product capsaicin partially alters the AURKA/PHB2 protein-protein proximity. We then synthesized 16 novel capsaicin analogues to enhance the effects of capsaicin. We found that replacing the long hydrophobic acyl moiety by a butyryl one increases the AURKA/PHB2 interaction. Among the capsaicin derivatives carrying this modification, we uncover that compound 13 enhances the AURKA/PHB2 proximity with a low experimental variability.

Together, our data indicate that compound 13 is a promising PHB ligand acting on the AURKA/PHB2 interaction, and it may provide the basis for the development of new anticancer drugs targeting the mitochondrial functions of AURKA.

Graphical abstract

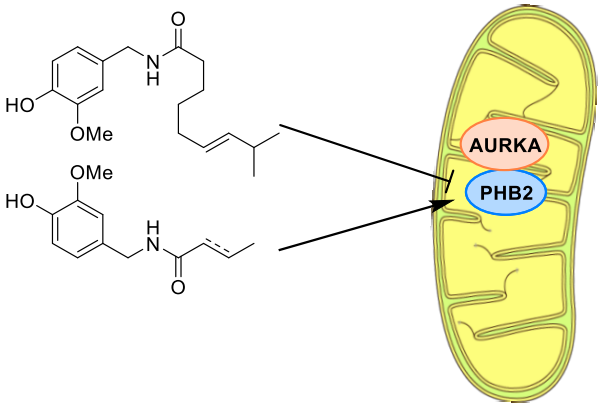

Highlights

- The cancer-related kinase Aurora A/AURKA interacts with the mitochondrial protein PHB2 to induce mitophagy in cancer cells
- Among the available PHB ligands, capsaicin mildly alters the AURKA/PHB2 interaction
- Screening of 16 newly-synthesized capsaicin derivatives show differential effects on the AURKA/PHB2 interaction
- Compound 13 significantly enhances the AURKA/PHB2 interaction and shows a low experimental variability

Introduction

Mitochondria are in constant equilibrium between turnover and biogenesis. To be able to metabolically sustain an uncontrolled cell proliferation in cancer cells, mitochondria are frequently hijacked to produce significant amounts of ATP[1]. In parallel, damaged mitochondria can be eliminated through a process called mitophagy[2,3]. Mitophagy is controlled by several proteins, including the scaffold protein Prohibitin-2 (PHB2) which binds to the autophagy mediator LC3[4]. PHB2 and its homolog Prohibitin-1 (PHB1) form a heterodimeric complex located on the Inner Mitochondrial Membrane (IMM), and constitute a hub for many signaling pathways beyond mitophagy in cancer cells[5].

Recently, the overexpression of the cancer-related protein Aurora kinase A/AURKA was shown to induce mitophagy by functionally interacting with PHB2[6]. AURKA regulates a wide variety of mitotic and non-mitotic functions at different subcellular compartments, including mitochondrial dynamics and ATP production[7–11]. We showed that AURKA phosphorylates PHB2 at Ser39 to induce the formation of an AURKA-LC3-PHB2 tripartite complex that triggers mitophagy in a PARK2/Parkin-independent manner[6]. AURKA-dependent mitophagy is used to eliminate defective mitochondria in cancer cells, while selecting a population of hyperfunctional organelles with high ATP production levels. We also found that the natural polyphenol xanthohumol acts as a PHB2 ligand on the inner membrane of mitochondria to destabilize the AURKA-LC3-PHB2 tripartite complex. By blocking the interaction between AURKA and LC3, treatment with xanthohumol results in mitophagy inhibition. Under these conditions, the AURKA-dependent mitochondrial ATP overproduction is also abolished, thereby linking an effective mitophagy and the capacity of mitochondria to increase their ATP production rates[6]. However, the polyphenolic structure of xanthohumol hampers its development as an anticancer agent.

As part of our ongoing programs on the development of new PHB ligands[12–16], we here screen already-available alternative PHB ligands in their capacity to alter the protein-protein interaction between AURKA and PHB2. We then optimize the activity of the most promising hit to obtain 16 novel ligands targeting the AURKA/PHB2 interaction. Last, we show that these ligands differentially affect the capacity of AURKA to interact with PHB2. Among these, we identify three new PHB ligands dramatically altering the interaction between AURKA and PHB2, becoming interesting candidates for follow-up studies.

Results

Screening of available PHB ligands identifies capsaicin as a compound lowering the interaction between AURKA and PHB2.

As an alternative to xanthohumol[6], we selected three PHB ligands with different chemical structures and with different functional consequences on PHB2 signaling pathways such as FL3, fluorizoline and capsaicin[5] (Figure 1).

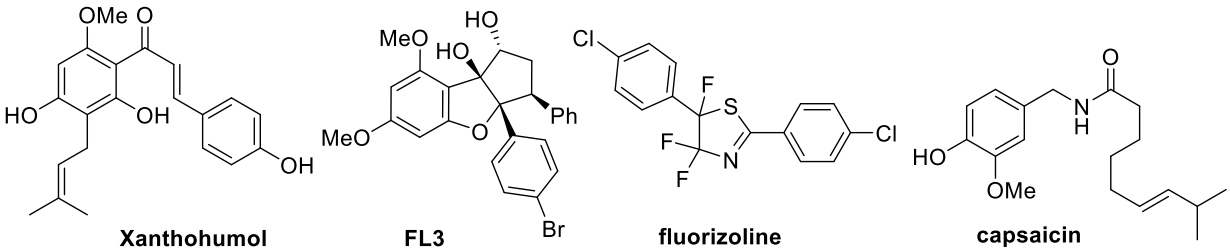

Figure 1: Structure of the PHB ligands xanthohumol, FL3, fluorizoline and capsaicin examined for their effects on the AURKA/PHB2 interaction in breast cancer cells.

We then compared the capacity of these three compounds to alter the protein-protein proximity between AURKA and PHB2 using Förster's Resonance Energy Transfer coupled to Fluorescence Lifetime Imaging Microscopy (FRET/FLIM) in live cells[6,17,18]. In these experiments, AURKA was fused to GFP and was used as a FRET donor, while PHB2 was fused to mCherry and was used as a FRET acceptor. FRET was represented using ∆Lifetime, which corresponds to the net difference between the lifetime of AURKA-GFP in the absence (AURKA-GFP + Empty vector, hereby donor-only condition) and in the presence of the acceptor (AURKA-GFP + PHB2-mCherry) (Figure 2). MCF7 breast cancer cells expressing AURKA-GFP in the presence or absence of PHB2-mCherry were incubated for 6h with each of the three compounds, or with the vehicle (DMSO) prior to FRET measurements.

Treatment with FL3 did not significantly impact the interaction between AURKA and PHB2 in FRET/FLIM analyses. In contrast, treatment with capsaicin or fluorizoline brought the ∆Lifetime of AURKA-GFP in the presence of PHB2-mCherry closer to that of their respective donor-only counterparts (Figure 2). This indicates that both compounds significantly lower the interaction between AURKA and PHB2. However, fluorizoline also displayed a significant green autofluorescence that made image-based analyses difficult. Thus, we selected capsaicin as a promising compound for the development of novel PHB ligands that could differentially modulate the AURKA/PHB2 interaction. Of note, capsaicin did not promote a nuclear localization of PHB2 in MCF7 cells, in contrast with a previous report in HeLa cells[19]. Our

FRET/FLIM analyses corroborate previous evidence, showing that PHB2 was exclusively localized at mitochondria in MCF7 cells[6].

Our data show that capsaicin mildly lowers the protein-protein interaction between AURKA and PHB2 at mitochondria. We next synthesized a series of new capsaicin derivatives, and we evaluated their effects on the AURKA/PHB2 interaction.

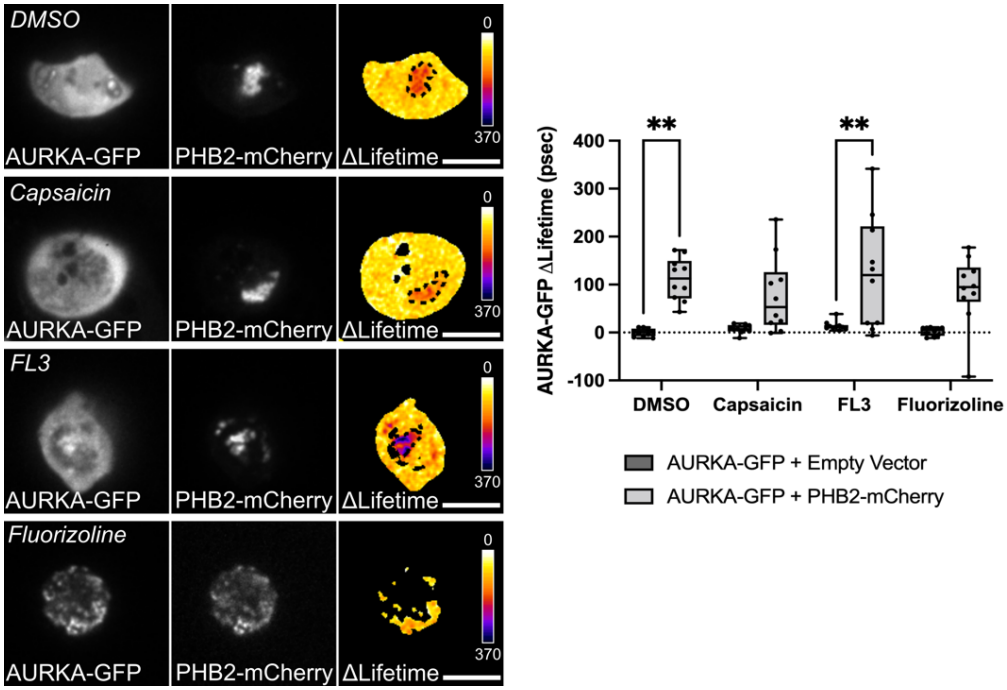

Figure 2: FRET/FLIM analyses on MCF7 cells expressing AURKA-GFP with an empty vector (donor-only condition), or with PHB2-mCherry. Cells were treated with vehicle (DMSO), capsaicin, FL3 or fluorizoline. Pseudocolour scale: pixel-by-pixel ΔLifetime. Graph: corresponding ΔLifetime quantifications performed in the dotted area. n = 10 cells per condition of one representative experiment (of three). Data extend from the min to the max. Dots indicate individual cells. Scale bar: 10 µm. *P<0.01 against each corresponding "AURKA-GFP + Empty vector" condition.

Chemical synthesis of novel capsaicin derivatives

After comparing several of methods of acylation, we found that Schotten-Baumann acylation allows the amine of vanillylamine **1a** to be selectively acylated without affecting the phenol as described by Short and coll. (Scheme 1)[20]. With this process, we synthesized 16 new capsaicin derivatives potentially behaving as PHB ligands (Figure 3). After the synthesis was completed, we then screened these compounds to explore whether they could alter the AURKA/PHB2 interaction at mitochondria.

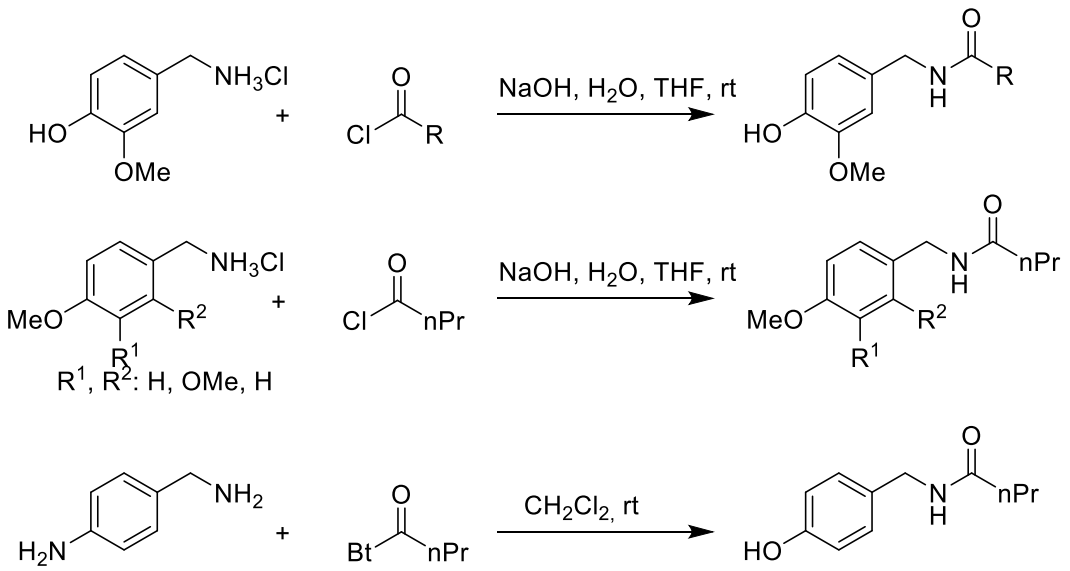

Scheme 1: Synthesis of capsaicin analogues.

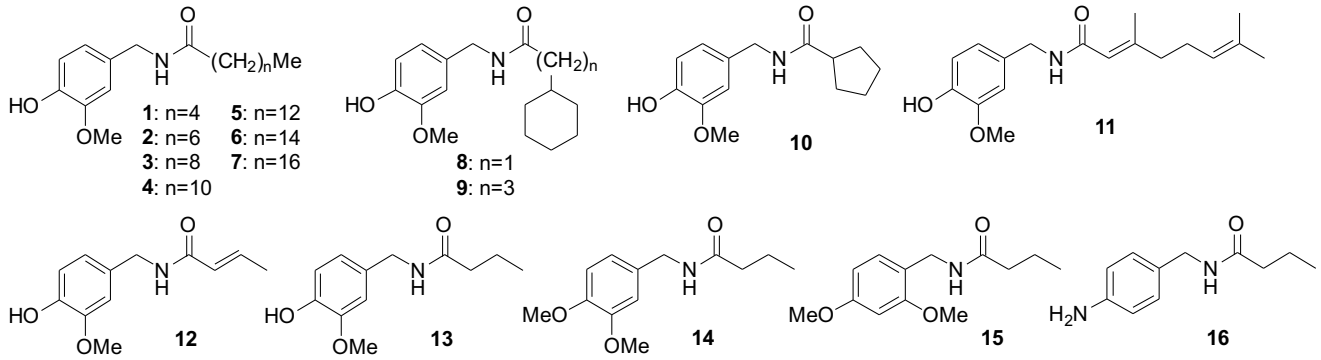

Figure 3: Structure of capsaicin analogues.

Capsaicin derivatives differentially affect the interaction between AURKA and PHB2.

To evaluate the effects of the 16 newly-synthesized capsaicin derivatives (Figure 3) towards the AURKA/PHB2 interaction, MCF7 cells expressing AURKA-GFP and PHB2-mCherry were treated for 6h with each capsaicin derivative or with the DMSO control compound, and their effects on the interaction between AURKA and PHB2 were evaluated using FRET/FLIM. The dynamic range of a GFP-mCherry chimeric tandem construct shows a maximum of 250 psec of ΔLifetime when compared to a GFP donor-only condition[17]. Given that the AURKA-GFP/PHB2-mCherry pair in the DMSO condition shows a mean ΔLifetime of 120-150 psec *per se*, we explored whether the 16 capsaicin derivatives could induce variations to these mean ΔLifetime values in cells co-expressing AURKA-GFP and PHB2-mCherry.

To this end, we calculated the mean ΔLifetime difference from the AURKA-GFP/PHB2-mCherry pair in the DMSO condition for each novel capsaicin derivative (Table 1). Variations

were considered mild when a given compound induced changes in the AURKA-GFP ΔLifetime of +/- 30-50 additional psec compared to what observed in the AURKA-GFP/PHB2-mCherry pair in the DMSO condition. This corresponds to 12-25% of the maximum ΔLifetime response of a GFP-mCherry tandem. Alternatively, variations were considered significant when a given compound induced changes in the AURKA-GFP ΔLifetime which were superior to +/- 50 additional psec compared to what observed in the AURKA-GFP/PHB2-mCherry pair in the DMSO condition. This is more than 25% of the maximum ΔLifetime response of a GFP-mCherry tandem.

The replacement of the acyl moiety of capsaicin by various linear and unsaturated fatty acids in compounds **1-7** (6 to 18 carbons) was detrimental to the FRET effect. Indeed, compounds **1**, **4**, **6** and **7** showed no effect on AURKA-GFP ΔLifetime when AURKA-GFP and PHB2-mcherry were co-expressed. Compounds **2**,**3** and **5** mildly lowered the AURKA/PHB2 interaction, but with a standard deviation superior to that of capsaicin (Table 1).

Compound	**Mean Δlifetime difference from DMSO (psec)**	**SD (psec)**	**Effect on the AURKA/PHB2 interaction**
Capsaicin	-41.92	14.1	Mildly lowered
1	-23.17	131.18	No significant variation
2	-48.26	85.25	Mildly lowered
3	-40.44	145.43	Mildly lowered
4	-2.93	109.07	No significant variation
5	-67.92	94.85	Mildly lowered
6	21.12	68.6	No significant variation
7	8.76	44.84	No significant variation
8	47.02	47.38	Mildly increased
9	48.96	63.07	Mildly increased
10	44.06	49.07	Mildly increased
11	74.89	77.81	Increased
12	77.09	79.45	Increased
13	66.35	13.97	Increased
14	12.87	55.99	No significant variation
15	0.77	24.93	No significant variation
16	51.92	63.9	Increased

Table 1. Effect of capsaicin derivatives on the AURKA/PHB2 interaction. Mean ΔLifetime differences and standard deviation (SD) of each capsaicin derivative when compared to the vehicle compound, in MCF7 cells co-expressing AURKA-GFP and PHB2-mCherry. Mild variations are between 30 and 50 psec, while variations are considered significant when they are more than 50 psec from the DMSO condition. Results are means from three independent experiments, with n = 10 cells per condition in each replicate.

Unexpectedly, the introduction of 5 or 6-membered ring in the hydrophobic acyl chain resulted in an opposite pharmacological activity. Indeed, the constrained analogues **8**, **9** and **10** mildly increased the interaction between AURKA and PHB2. Of note, this compounds also show a lower degree of experimental variability than the previously-tested compounds in our FRET/FLIM analyses (Table 1). Similarly to compounds **8-10**, *N*-vanillylgeranamide/compound **11** displayed some rigidification as well. However, this compound promoted AURKA/PHB2 interaction to a greater extent than the previous analogues (Table 1). Shortening the hydrophobic chain into a crotonic group as in compound **12** also induced significant changes of more than 50 psec in AURKA-GFP ΔLifetime, thus increasing the interaction between AURKA and PHB2 compared to that observed in the DMSO condition (Figure 4A, Table 1). Nevertheless, both compounds **11** and **12** displayed a high standard deviation. Switching to the more flexible butyryl group as in compound **13** was another suitable strategy to significantly increase the AURKA/PHB2 interaction. Furthermore, compound **13** displayed a much lower standard deviation than compound **11** or **12** (Figure 4B, Table 1). Thus, we chose to modify this analogue to explore the vanillyl moiety.

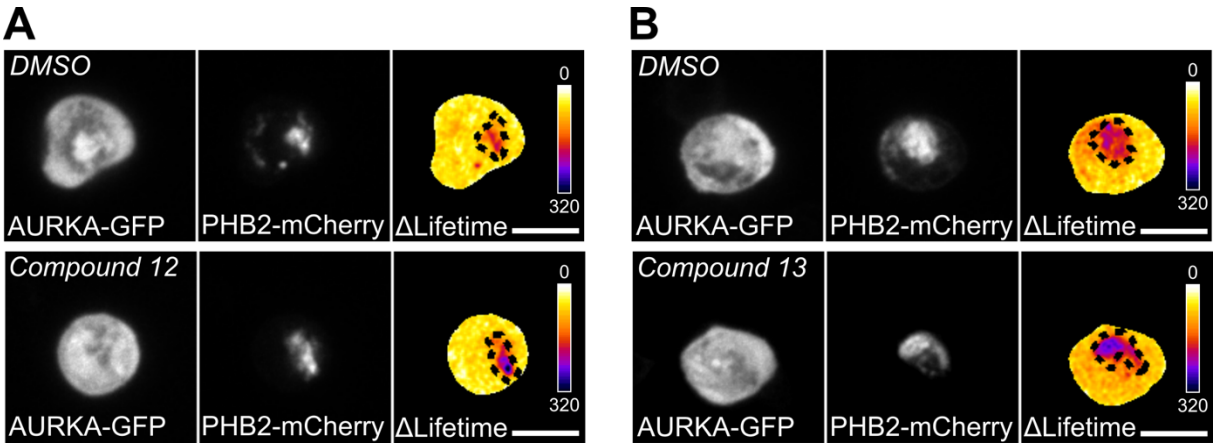

Figure 4: FRET/FLIM analyses on MCF7 cells co-expressing AURKA-GFP (donor) and PHB2-mCherry (acceptor). Cells were treated with vehicle (DMSO), **13** (A) or **12** (B). Pseudocolour scale: pixel-by-pixel ΔLifetime. Dotted area: PHB2-rich mitochondrial area. Scale bar: 10 µm.

The methylation of the phenolic moiety as in compound **14** and **15** left the interaction between AURKA and PHB2 unaltered. On the contrary, its replacement by an aniline as in compound **16** increased the interaction between the two proteins (Table 1). This indicates the requirement for a H-bond donor in this position.

To exclude that the capsaicin derivatives could significantly perturb the lifetime of AURKA-GFP *per se,* each compound was evaluated in the donor-only condition where AURKA-GFP was co-expressed with an empty vector (Table 2). Previous reports demonstrated that a ΔLifetime difference below 50 psec corresponds to the standard deviation of our FLIM setup[17,18]. Therefore, a difference in the AURKA-GFP ΔLifetime above 50 psec may indicate that the tested ligands intrinsically affect the lifetime of AURKA-GFP, and this beyond the FRET effect. Globally, the majority of the compounds tested showed a non-significant variation

of ΔLifetime in the donor-only condition. Nevertheless, we observed that compound **16** shows a slightly higher variability than the other derivatives under these conditions. This suggest that the differences in ΔLifetime observed upon the co-expression of AURKA-GFP and PHB2-mCherry (Table 1) in cells treated with compound **16** could be partially independent of the FRET effect and could be explained with an intrinsic effect of the compound **16** on the donor lifetime.

Compound	**Mean Δlifetime difference from DMSO (psec)**	**SD (psec)**
Capsaicin	5.22	12.03
1	21.95	52.61
2	17.95	50.59
3	4.49	40.04
4	14.01	45.02
5	7.46	39.17
6	28.72	40.49
7	30.9	20.29
8	10.17	57.25
9	7.85	69.3
10	17.98	35.75
11	34.54	17.48
12	48.45	39.74
13	50.73	42.45
14	8.87	7.71
15	19.95	21.42
16	55.98	51.84

Table 2. Effect of capsaicin and its derivatives on the AURKA-GFP lifetime. Mean ΔLifetime differences and standard deviation (SD) of each capsaicin derivative when compared to the vehicle (DMSO), in MCF7 cells expressing AURKA-GFP and an empty vector. Results are means from three independent experiments, with n = 10 cells per condition in each replicate.

In conclusion, our results show that our newly-generated capsaicin derivatives differentially modulate the interaction between AURKA and PHB2 at mitochondria in live cells. While the majority had either no effect or a mild effect on this interaction, we determined that compounds **11**, **12** and **13** significantly increase the AURKA/PHB2 protein-protein proximity. Among these, compound **13** increases the AURKA/PHB2 interaction combined with a low standard deviation. Together, this makes of this capsaicin derivative the most promising hit among the 16 compounds here generated.

Discussion

Aurora kinase A/AURKA is a hallmark of epithelial and hematological cancers, where it is frequently overexpressed both at the mRNA or at the protein level[8]. It is known that AURKA has multiple subcellular locations, including mitochondria[9,10].

We here identified capsaicin as a PHB2 ligand that lowers the AURKA/PHB2 interaction at mitochondria. This compound was previously shown to induce a dissociation between PHB and the Adenine Nucleotide Translocator 2 (ANT2, SLC25A5). Proteomics studies suggest that the auto/mitophagy modulator LC3 may interact with ANT2 and in our previous study, we identified ANT2 as an interactor of AURKA using MS/MS-based approaches[9]. In addition, we previously observed that AURKA interacts with LC3 in a PHB2-dependent manner[6]. This raises the interesting possibility that PHB2, AURKA ANT2 and LC3 may form a quaternary complex in mitochondria.

Capsaicin is known to be cytotoxic in a wide range of cancer cell lines. Beyond PHB2[19], these effects have been attributed to the action of capsaicin on several targets. These include the neuronal vanilloid receptor TRPV1[21,22], the Tumor-Associated NADH Oxidase class (tNOX/ENOX2) protein, which is ubiquitously expressed in cancer but not in non-transformed cells[23], the nuclear lysine specific demethylase 1A (KDM1A/LSD1)[24], and the nuclear transcription factor 2 (POU3F2)[25]. Capsaicin was shown to bind to PHB2, and to induce its translocation from the inner mitochondrial membrane to the nucleus in HeLa cells[19]. This also contributes to the induction of apoptosis in human myeloid leukemia cells. Given these multiple targets of capsaicin, it is interesting to note that compound **13** is unable to significantly activate TRPV1[26]. This potentially makes of compound **13** a more selective PHB ligand than capsaicin. Despite these multiple targets of capsaicin, it is important to note that they are not localized at mitochondria and that the effect of capsaicin at this subcellular compartment was still unknown. We here provide the first evidence for the capacity of capsaicin and its derivatives to modulate the protein/protein proximity between PHB2 and a cancer-related kinase such as AURKA at this compartment.

At mitochondria, AURKA was shown to play a variety of roles including the modulation of mitochondrial morphology, of ATP production and of mitochondrial clearance by mitophagy[6,9]. We showed that the PHB2 ligand xanthohumol globally alters protein-protein interactions within the AURKA-PHB2-LC3 tripartite complex. Indeed, xanthohumol lowers the AURKA/LC3 interaction while concomitantly increasing the AURKA/PHB2 interaction. Altering these interactions abolishes AURKA-dependent mitophagy and restores normal ATP levels in cancer cells with AURKA overexpression[6]. When looking at the newly-generated capsaicin derivatives, it is interesting to observe that compounds **11**, **12** and **13** significantly increase the AURKA/PHB2 interaction as xanthohumol does[6].

Thanks to its low standard deviation compared to those of compounds **11** and **12**, our data suggest that compound **13** is a promising capsaicin derivative for follow-up studies in AURKA-overexpressing cancers. Future reports will elucidate whether the AURKA/PHB2 interaction could be considered as a proxy to predict the efficacy of capsaicin derivatives towards the mitochondrial functions of AURKA and ultimately, the proliferation rates of cancer cells. Our study paves the way to the use of capsaicin derivatives to be used as lead compounds towards the development of a new class of anticancer drugs.

Materials and methods

CHEMICAL SYNTHESIS

General procedure A for the acylation of vanillylamine

The acyl chloride (3.3 mmol) was added dropwise to a solution of vanillylamine hydrochloride (0.569 g, 3.0 mmol) of sodium hydroxide (0.24 g, 6 mmol) in water (1.2 ml) and THF (1 ml) at 0°C under stirring. After 5 min, the medium was stirred at rt for 2 h, concentrated in vacuo, quenched with 1N HCl and extracted with Et_2O. The organic layers were combined, washed with a saturated solution of Na_2SO_4, dried ($MgSO_4$) and concentrated under vacuum. The residue was purified by flash chromatography on silica gel using first Et_2O or Et_2O/DCM (2:8) and then AcOEt.

General procedure B for the acylation of vanillylamine

A mixture of the acid (0.8 mmol), HOBt (108 mg), vanillylamine hydrochloride (151 mg, 0.8 mmol) and triethylamine (82 mg, 0.8 mmol) in 3 ml of anhydrous DMF was cooled down to 0°C under stirring. After 10 minutes, EDCI (173 mg, 0.9 mmol) was added and stirred overnight at room temperature. The medium was the diluted with water, extracted with Et_2O (2X), washed with HCl (1M), a saturated solution of $NaHCO_3$, a saturated solution of Na_2SO_4, filtered, concentrated under vacuum. The residue was purified by flash chromatography on silica gel using first CH_2Cl_2/pentane 1:1 to 1:0 and then with CH_2Cl_2/ Et_2O 8:2 if necessary to afford the expected amide.

N-(4-Hydroxy-3-methoxybenzyl)hexanamide (1)

Following the general procedure A, the amide **1** was obtained in 62 % yield (0.467 g). ^{1}H NMR (500 MHz, $CDCl_3$) δ 6.91 – 6.68 (m, 3H), 5.90 (s, 2H), 4.33 (d, *J* = 5.7 Hz, 2H), 3.86 (s, 3H), 2.27 – 2.10 (m, 2H), 1.70 – 1.55 (m, 2H), 1.30 (d, *J* = 3.6 Hz, 4H), 0.90 – 0.79 (m, 3H). ^{13}C NMR (126 MHz, $CDCl_3$) δ 173.16, 146.86, 145.24, 130.43, 120.83, 114.52, 110.82, 56.00, 43.59, 36.88, 31.57, 25.58, 22.49, 14.03.

N-(4-Hydroxy-3-methoxybenzyl)octanamide (2)

Following the general procedure A, the amide **2** was obtained in 34 % yield (0.285 g). ^{1}H NMR (500 MHz, $CDCl_3$) δ 6.93 – 6.69 (m, 3H), 5.79 (s, 2H), 4.35 (d, *J* = 5.7 Hz, 2H), 3.87 (s, 3H), 2.26 – 2.12 (m, 2H), 1.64 (qd, *J* = 7.6, 3.6 Hz, 2H), 1.38 – 1.19 (m, 8H), 0.93 – 0.80 (m, 3H). 13C NMR (126 MHz, CDCl3) δ 173.10, 146.85, 145.25, 130.48, 120.89, 114.51, 110.82, 77.36, 56.03, 43.63, 36.97, 31.80, 29.38, 29.12, 25.91, 22.71, 14.17.

N-(4-Hydroxy-3-methoxybenzyl)decanamide (3)

Following the general procedure B, the amide **3** was obtained in 37 % yield (90 mg). ^{1}H NMR (500 MHz, $CDCl_3$) δ 6.91 – 6.72 (m, 3H), 4.36 (d, *J* = 5.6 Hz, 2H), 3.89 (s, 3H), 2.30 – 2.11 (m, 2H), 1.68-1.62 (m, 2H), 1.38 – 1.14 (m, 12H), 0.94 – 0.80 (m, 3H). ^{13}C NMR (126 MHz, $CDCl_3$) δ 172.98, 146.78, 145.22, 130.53, 120.93, 114.45, 110.78, 77.33, 56.04, 43.64, 37.00, 31.97, 29.56, 29.47, 29.43, 29.37, 25.90, 22.77, 14.21.

***N*-(4-Hydroxy-3-methoxybenzyl)dodecanamide (4)**

Following the general procedure B, the amide **4** was obtained in 52 % yield (140 mg). ^{1}H NMR (500 MHz, $CDCl_3$) δ 6.95 – 6.69 (m, 3H), 4.37 (d, *J* = 5.7 Hz, 2H), 3.89 (s, 3H), 2.20 (t, *J* = 7.6 Hz, 2H), 1.66 (p, *J* = 7.4 Hz, 2H), 1.58 (s, 2H), 1.26 (s, 14H), 0.89 (t, *J* = 6.9 Hz, 3H). ^{13}C NMR (126 MHz, $CDCl_3$) δ 173.01, 146.82, 145.26, 130.58, 120.97, 114.48, 110.81, 56.08, 43.68, 37.04, 32.05, 29.75, 29.64, 29.51, 29.47, 25.94, 22.83, 14.26.

***N*-(4-Hydroxy-3-methoxybenzyl)tetradecanamide (5)**

Following the general procedure B, the amide **5** was obtained in 68 % yield (197 mg). ^{1}H NMR (500 MHz, $CDCl_3$) δ 6.89 – 6.69 (m, 3H), 5.63 (s, 1H), 4.37 (d, *J* = 5.6 Hz, 2H), 3.89 (s, 3H), 2.20 (t, *J* = 7.6 Hz, 2H), 1.69 – 1.61 (m, 2H), 1.26 (d, *J* = 3.1 Hz, 20H), 0.89 (t, *J* = 6.8 Hz, 3H). ^{13}C NMR (126 MHz, $CDCl_3$) δ 173.02, 146.82, 145.26, 130.57, 120.97, 114.48, 110.81, 56.09, 43.68, 37.04, 32.07, 29.82, 29.79, 29.76, 29.65, 29.51, 29.50, 29.48, 25.94, 22.84, 14.27.

***N*-(4-Hydroxy-3-methoxybenzyl)palmitamide (6)**

Following the general procedure B, the amide **6** was obtained in 48 % yield (148 mg). ^{1}H NMR (500 MHz, $CDCl_3$) δ 6.92 – 6.72 (m, 3H), 5.61 (d, *J* = 19.9 Hz, 2H), 4.37 (d, *J* = 5.6 Hz, 2H), 3.89 (s, 3H), 2.20 (t, *J* = 7.6 Hz, 2H), 1.66 (p, *J* = 7.5 Hz, 2H), 1.34 – 1.22 (m, 24H). ^{13}C NMR (126 MHz, $CDCl_3$) δ 173.01, 146.82, 145.25, 130.57, 120.97, 114.48, 110.81, 77.36, 56.09, 43.68, 37.05, 32.08, 29.85, 29.82, 29.80, 29.76, 29.65, 29.51, 29.48, 25.94, 22.84, 14.27.

***N*-(4-Hydroxy-3-methoxybenzyl)stearamide (7)**

Following the general procedure B, the amide **7** was obtained in 81 % yield (270 mg). ^{1}H NMR (500 MHz, $CDCl_3$) δ 6.93 – 6.68 (m, 3H), 5.59 (s, 2H), 4.37 (d, *J* = 5.6 Hz, 2H), 3.89 (s, 3H), 2.26 – 2.13 (m, 2H), 1.66 (p, *J* = 7.6 Hz, 2H), 1.26 (d, *J* = 4.0 Hz, 28H), 0.89 (t, *J* = 6.9 Hz, 3H). ^{13}C NMR (126 MHz, $CDCl_3$) δ 13C NMR (126 MHz, CDCl3) δ 173.02, 146.82, 145.26, 130.58, 120.98, 114.49, 110.81, 56.09, 43.69, 37.05, 32.08, 29.85, 29.83, 29.81, 29.76, 29.65, 29.51, 29.48, 25.94, 22.84, 14.27.

2-Cyclohexyl-*N*-(4-hydroxy-3-methoxybenzyl)acetamide (8)

Following the general procedure B, the amide **8** was obtained in 32 % yield (89 mg). ^{1}H NMR (500 MHz, $CDCl_3$) δ 6.93 – 6.69 (m, 3H), 5.60 (s, 2H), 4.37 (d, *J* = 5.7 Hz, 2H), 3.88 (s, 3H), 2.07 (d, *J* = 7.1 Hz, 2H), 1.84 (d, *J* = 33.1 Hz, 1H), 1.79 – 1.73 (m, 2H), 1.68 (d, *J* = 34.5 Hz, 3H), 1.37 – 1.20 (m, 3H), 1.20 – 1.07 (m, 1H), 1.01 – 0.88 (m, 2H). ^{13}C NMR (126 MHz, $CDCl_3$) δ 172.27, 146.83, 145.23, 130.62, 120.93, 114.46, 110.75, 77.36, 56.05, 45.14, 43.62, 35.57, 33.34, 26.34, 26.20.

3-Cyclohexyl-*N*-(4-hydroxy-3-methoxybenzyl)propanamide (9)

Following the general procedure B, the amide **9** was obtained in 33 % yield (80 mg). ^{1}H NMR (500 MHz, $CDCl_3$) δ 6.96 – 6.62 (m, 3H), 5.64 (br s, 1H), 5.60 (s, 1H), 4.36 (d, *J* = 5.6 Hz, 2H), 3.89 (s, 3H), 2.18 (t, *J* = 7.6 Hz, 2H), 1.77 – 1.60 (m, 7H), 1.33 – 1.04 (m, 6H). ^{13}C NMR (126 MHz, $CDCl_3$) δ 173.02, 146.82, 145.26, 130.58, 120.98, 114.49, 110.83, 56.09, 43.68, 37.60, 37.31, 37.20, 33.42, 26.79, 26.75, 26.48, 23.31.

***N*-(4-Hydroxy-3-methoxybenzyl)cyclopentanecarboxamide (10)**

Following the general procedure B, the amide **10** was obtained in 27 % yield (11 mg). ^{1}H RMN (500 MHz, $CDCl_3$) δ 6.86 (s, 1H), 6.81 (d, *J* = 2.0 Hz, 2H), 6.78 (d, *J* = 2.0 Hz, 1H), 4.37 (d, *J* = 5.6 Hz, 2H), 3.89 (s, 3H), 2.52 (d, *J* = 8.2 Hz, 1H), 1.90 - 1,74 (m, 4H), 1.66 – 1.52 (m, 4H). ^{13}C RMN (126 MHz, $CDCl_3$) δ 176.13, 146.81, 145.21, 130.70, 120.88, 114.49, 110.75, 56.08, 46.09, 43.68, 30.61, 26.06.

***N*-(4-Hydroxy-3-methoxybenzyl)-3,7-dimethylocta-2,6-dienamide (11)**

Following the general procedure B, the amide **11** was obtained in 52 % yield (252 mg). ^{1}H NMR (500 MHz, $CDCl_3$) δ 6.94 – 6.70 (m, 3H), 5.64 (d, *J* = 19.7 Hz, 2H), 5.07 (ddddt, *J* = 7.4, 5.9, 4.4, 2.9, 1.4 Hz, 1H), 4.41 – 4.31 (m, 2H), 2.31 – 2.01 (m, 5H), 1.77 – 1.51 (m, 6H). ^{13}C NMR (126 MHz, $CDCl_3$) δ 167.21, 155.01, 147.06, 145.45, 132.74, 132.66, 130.92, 124.23, 123.57, 121.25, 121.23, 119.45, 118.21, 114.74, 114.71, 111.13, 111.11, 77.62, 56.34, 56.32, 43.67, 41.16, 33.53, 27.06, 26.49, 26.06, 26.03, 25.10, 18.77, 18.08, 18.04.

(E)-*N*-(4-hydroxy-3-methoxybenzyl)but-2-enamide (12)

Following the general procedure A, the amide **12** was obtained in 11 % yield (70 mg). ^{1}H RMN (500 MHz, $CDCl_3$) δ 6.88 (s, 1H), 6.86 (s, 1H), 6.83 (d, *J* = 1.9 Hz, 1H), 6.79 (dd, *J* = 8.0, 1.9 Hz, 1H), 5.80 (dq, *J* = 15.1, 1.7 Hz, 1H), 5.60 (s, 1H), 4.43 (d, *J* = 5.7 Hz, 2H), 3.89 (s, 2H), 1.87 (dd, *J* = 6.9, 1.7 Hz, 2H). ^{13}C RMN (126 MHz, $CDCl_3$) δ 165.55, 146.58, 145.03, 140.21, 130.16, 124.77, 120.80, 114.24, 110.62, 55.86, 43.44, 17.64.

***N*-(4-Hydroxy-3-methoxybenzyl)butyramide (13)**

Following the general procedure A, the amide **13** was obtained in 68 % yield (457 mg). ^{1}H NMR (500 MHz, $CDCl_3$) δ 6.87 (d, *J* = 8.0 Hz, 1H), 6.81 (d, *J* = 2.0 Hz, 1H), 6.77 (dd, *J* = 8.0, 2.0 Hz, 1H), 5.67 (s, 1H), 4.36 (d, *J* = 5.6 Hz, 2H), 3.88 (s, 3H), 2.18 (d, *J* = 7.5 Hz, 2H), 1.75 – 1.64 (m, 2H), 0.96 (t, *J* = 7.5 Hz, 3H). ^{13}C NMR (126 MHz, $CDCl_3$) δ 172.62, 146.58, 145.00, 130.28, 120.68, 114.24 110.56, 55.82, 43.40, 38.63, 19.07, 13.66.

***N*-(4-Hydroxy-3-methoxybenzyl)butanamide (14)**

Starting with (3,4-dimethoxyphenyl)methanamine and following the general procedure A, the amide **14** was obtained in 16 % yield (113 mg). ^{1}H NMR (500 MHz, $CDCl_3$) δ 6.83 (s, 3H), 4.39 (d, *J* = 5.7 Hz, 2H), 3.88 (s, 6H), 2.20 (t, J = 7.5 Hz, 2H), 1.70 (sex, J = 7.5 Hz, 2H), 0.97 (t, J = 7.5 Hz, 3H). ^{13}C NMR (126 MHz, $CDCl_3$) δ 172.60, 149.07, 148.38, 130.95, 119.99, 111.10, 111.06, 55.85, 55.78, 43.31, 38.65, 19.09, 13.68.

***N*-(2,4-Dimethoxybenzyl)butyramide (15)**

Starting with (2,4-dimethoxyphenyl)methanamine and following the general procedure A, the amide **15** was obtained in 37 % yield (0.264 mg). ^{1}H NMR (500 MHz, $CDCl_3$) δ 7.19 (d, *J* = 8.1 Hz, 1H), 6.46 (d, *J* = 2.4 Hz, 1H), 6.44 (dd, *J* = 8.1, 2.4 Hz, 1H), 4.37 (d, *J* = 5.7 Hz, 2H), 4.38 (s, 3H), 4.37 (s, 3H), 2.14 (t, *J* = 7.5 Hz, 2H), 1.66 (sex, *J* = 7.5 Hz, 2H), 0.93 (t, *J* = 7.5 Hz, 3H). ^{13}C NMR (126 MHz, $CDCl_3$) δ 172.35, 160.38, 158.46, 130.51, 118.89, 103.79, 98.49, 55.28, 55.21, 38.77, 38.69, 19.01, 13.62.

***N*-(4-Aminobenzyl)butyramide (16)**

1-Butyroyl-1H-benzotriazole (0.567 g, 3 mmol) and 4-(aminomethyl)aniline (0.366 g, 3 mmol) were stirred in dichloromethane (10 mL) at room temperature for one night. The solvent was replaced by Et_2O. The organic layer was washed with a solution of K_2HPO_4 and $NaHCO_3$, dried over Na_2SO_4 and concentrated. The oil was purified by column chromatography (Et_2O and AcOEt) and concentrated under vacuum to give the title amide in 37 % yield (0.264 mg) as a pale-yellow powder. ^{1}H NMR (500 MHz, $CDCl_3$) δ 7.05 (d, *J* = 8.4 Hz, 2H), 6.62 (d, *J* = 8.3 Hz, 2H), 5.81 (s, 1H), 4.29 (d, *J* = 5.5 Hz, 1H), 3.69 (s, 2H), 2.15 (t, J = 7.4 Hz 2H), 1.66 (quint, *J* = 7.4 Hz, 1H), 0.93 (t, *J* = 7.4 Hz, 3H). ^{13}C NMR (126 MHz, $CDCl_3$) δ 172.57, 145.71, 128.95 (2C), 127.99, 115.00 (2C), 60.22, 43.02, 38.52, 19.01, 13.61.

IN CELLULO ANALYSES

Cell culture procedures

MCF7 (HTB-22) cells were purchased from the American Type Culture Collection and were kept free from mycoplasma throughout experiments. They were grown in Dulbecco's Modified Eagle's Medium (DMEM) already containing 1% L-glutamine (Thermo Fisher Scientific), and supplemented with 10% FBS (Thermo Fisher Scientific) and 1% penicillin– streptomycin (Thermo Fisher Scientific). For all live microscopy experiments, cells were grown at 37°C either in Nunc Lab-Tek Chamber slides (Thermo Fisher Scientific), or in polymer-coated µ-Slide 8 Well high slides (Ibidi). Before proceeding with FLIM imaging, standard growth media was replaced with phenol red-free Leibovitz's L-15 medium (Thermo Fisher Scientific) supplemented with 20% FBS and 1% penicillin–streptomycin. Plasmid transfections were performed with Lipofectamine 2000 (Thermo Fisher Scientific), according to the manufacturer's instructions and incubated for 48h before FLIM analyses. pcDNA3 AURKA-GFP, a pcDNA 3.1 empty vector and pmCherry N1 PHB2 were previously described[6].

Fluorizoline, FL3, capsaicin and all capsaicin derivatives were resuspended in DMSO and stored at -20°C for long-term storage. Each compound was used at a final concentration of 10 µM, and incubated for 6h before proceeding with microscopy experiments.

FLIM microscopy

For FLIM analyses, images were acquired with a time-gated custom-made setup based on a spinning disk microscope as described in [18]. GFP was used as a FRET donor in all experiments, and it was excited at 480 ± 10 nm with a supercontinuum picosecond pulsed laser source. Emission was selected using a band pass filter of 483/35 nm. The FLIM setup

was controlled by the Inscoper Suite solution (Inscoper, France), and GFP lifetime was measured in real-time during acquisition with the Inscoper software. In all experiments, AURKA-GFP lifetime was calculated by the Inscoper software only when the pixel- by-pixel fluorescence intensity in the first gate was above 2000 gray levels. To calculate the ΔLifetime, the mean lifetime of the cells in the donor-only condition (AURKA-GFP + Empty vector) was calculated, and then used to normalize data in all the analyzed conditions and for each independent experiment as previously reported[27].

Statistical analyses

Two-way ANOVA was used to compare the effect of the transfection conditions and of the pharmacological treatments (Fig. 2), and was performed using GraphPad Prism v. 10. Statistics and summary statistics for biological replicates comparing the effect of the transfection conditions and the pharmacological treatments were performed with SuperPlotsofData[28] (Tables 1, 2).

Author contributions

CRediT taxonomy: Conceptualization (G.B., L.D.), Data Curation (A.D., C.C., V.P., K.F., G.B., L.D.), Formal Analysis (A.D., C.C., V.P., K.F., G.B., L.D.), Funding Acquisition (G.B., L.D.), Investigation (A.D., C.C., V.P., K.F., G.B., L.D.), Methodology (G.B., L.D.), Project Administration (G.B., L.D.), Resources (G.B., L.D.), Software (C.C., V.P., G.B.), Supervision (G.B., L.D.), Validation (G.B., L.D.), Visualization (C.C., V.P., G.B., L.D.), Writing – original, review and editing (C.C., G.B., L.D.).

Acknowledgements

We thank S. Dutertre, X. Pinson and G. Le Marchand at the Microscopy Rennes Imaging Center (MRic, *Biologie, Santé, Innovation Technologique*_- BIOSIT, Rennes, France) for assistance with FLIM experiments. MRic is member of the national infrastructure France-BioImaging, supported by the French National Research Agency (ANR-10-INBS-04). This work was supported by the Centre National de la Recherche Scientifique (CNRS), the University of Rennes, the *Ligue Contre le Cancer, Comités d'Ille et Vilaine et du Finistère* to G.B. C.C was supported by a PhD fellowship from the Ligue Nationale Contre le Cancer (grant no. IP/SC – 17653).

Competing interests

The authors declare no competing or financial interests.

References

1. Wang, T., Ma, F., and Qian, H. (2021). Defueling the cancer: ATP synthase as an emerging target in cancer therapy. Molecular Therapy - Oncolytics *23*, 82–95. https://doi.org/10.1016/j.omto.2021.08.015.

2. Pickrell, A.M., and Youle, R.J. (2015). The Roles of PINK1, Parkin and Mitochondrial Fidelity in Parkinson's Disease. Neuron *85*, 257–273. https://doi.org/10.1016/j.neuron.2014.12.007.

3. Wang, S., Long, H., Hou, L., Feng, B., Ma, Z., Wu, Y., Zeng, Y., Cai, J., Zhang, D., and Zhao, G. (2023). The mitophagy pathway and its implications in human diseases. Sig Transduct Target Ther *8*, 1–28. https://doi.org/10.1038/s41392-023-01503-7.

4. Wei, Y., Chiang, W.-C., Sumpter, R., Mishra, P., and Levine, B. (2017). Prohibitin 2 Is an Inner Mitochondrial Membrane Mitophagy Receptor. Cell *168*, 224-238.e10. https://doi.org/10.1016/j.cell.2016.11.042.

5. Wang, D., Tabti, R., Elderwish, S., Abou-Hamdan, H., Djehal, A., Yu, P., Yurugi, H., Rajalingam, K., Nebigil, C.G., and Désaubry, L. (2020). Prohibitin ligands: a growing armamentarium to tackle cancers, osteoporosis, inflammatory, cardiac and neurological diseases. Cell. Mol. Life Sci. *77*, 3525–3546. https://doi.org/10.1007/s00018-020-03475-1.

6. Bertolin, G., Alves-Guerra, M.-C., Cheron, A., Burel, A., Prigent, C., Borgne, R.L., and Tramier, M. (2021). Mitochondrial Aurora kinase A induces mitophagy by interacting with MAP1LC3 and Prohibitin 2. Life Science Alliance *4*. https://doi.org/10.26508/lsa.202000806.

7. Kashatus, D.F., Lim, K.-H., Brady, D.C., Pershing, N.L.K., Cox, A.D., and Counter, C.M. (2011). RALA and RALBP1 regulate mitochondrial fission at mitosis. Nature Cell Biology *13*, 1108–1115. https://doi.org/10.1038/ncb2310.

8. Nikonova, A.S., Astsaturov, I., Serebriiskii, I.G., Dunbrack, R.L., and Golemis, E.A. (2013). Aurora A kinase (AURKA) in normal and pathological cell division. Cellular and Molecular Life Sciences *70*, 661–687. https://doi.org/10.1007/s00018-012-1073-7.

9. Bertolin, G., Bulteau, A.-L., Alves-Guerra, M.-C., Burel, A., Lavault, M.-T., Gavard, O., Le Bras, S., Gagné, J.-P., Poirier, G.G., Le Borgne, R., et al. (2018). Aurora kinase A localises to mitochondria to control organelle dynamics and energy production. eLife *7*. https://doi.org/10.7554/eLife.38111.

10. Grant, R., Abdelbaki, A., Bertoldi, A., Gavilan, M.P., Mansfeld, J., Glover, D.M., and Lindon, C. (2018). Constitutive regulation of mitochondrial morphology by Aurora A kinase depends on a predicted cryptic targeting sequence at the N-terminus. Open Biology *8*, 170272. https://doi.org/10.1098/rsob.170272.

11. Bertolin, G., and Tramier, M. (2020). Insights into the non-mitotic functions of Aurora kinase A: more than just cell division. Cell. Mol. Life Sci. *77*, 1031–1047. https://doi.org/10.1007/s00018-019-03310-2.

12. Chouha, N., Abou-Hamdan, H., Yurugi, H., Yoshii, R., Ii, H., Najem, A., Ghanem, G.E., Nakata, S., Rajalingam, K., Peng, Y., et al. (2022). Development of fluorizoline analogues as prohibitin ligands that modulate C-RAF signaling, p21 expression and melanogenesis. European Journal of Medicinal Chemistry *242*, 114635. https://doi.org/10.1016/j.ejmech.2022.114635.

13. Tabti, R., Lamoureux, F., Charrier, C., Ory, B., Heymann, D., Bentouhami, E., and

Désaubry, L. (2021). Development of prohibitin ligands against osteoporosis. European Journal of Medicinal Chemistry *210*, 112961. https://doi.org/10.1016/j.ejmech.2020.112961.

14. Yurugi, H., Zhuang, Y., Siddiqui, F.A., Liang, H., Rosigkeit, S., Zeng, Y., Abou-Hamdan, H., Bockamp, E., Zhou, Y., Abankwa, D., et al. (2020). A subset of flavaglines inhibits KRAS nanoclustering and activation. Journal of Cell Science *133*, jcs244111. https://doi.org/10.1242/jcs.244111.

15. Elderwish, S., Audebrand, A., Nebigil, C.G., and Désaubry, L. (2020). Discovery of 3,3′-pyrrolidinyl-spirooxindoles as cardioprotectant prohibitin ligands. European Journal of Medicinal Chemistry *186*, 111859. https://doi.org/10.1016/j.ejmech.2019.111859.

16. Djehal, A., Krayem, M., Najem, A., Hammoud, H., Cresteil, T., Nebigil, C.G., Wang, D., Yu, P., Bentouhami, E., Ghanem, G.E., et al. (2018). Targeting prohibitin with small molecules to promote melanogenesis and apoptosis in melanoma cells. European Journal of Medicinal Chemistry *155*, 880–888. https://doi.org/10.1016/j.ejmech.2018.06.052.

17. Padilla-Parra, S., Audugé, N., Coppey-Moisan, M., and Tramier, M. (2008). Quantitative FRET analysis by fast acquisition time domain FLIM at high spatial resolution in living cells. Biophys. J. *95*, 2976–2988. https://doi.org/10.1529/biophysj.108.131276.

18. Leray, A., Padilla-Parra, S., Roul, J., Héliot, L., and Tramier, M. (2013). Spatio-Temporal Quantification of FRET in living cells by fast time-domain FLIM: a comparative study of non-fitting methods [corrected]. PLoS ONE *8*, e69335. https://doi.org/10.1371/journal.pone.0069335.

19. Kuramori, C., Azuma, M., Kume, K., Kaneko, Y., Inoue, A., Yamaguchi, Y., Kabe, Y., Hosoya, T., Kizaki, M., Suematsu, M., et al. (2009). Capsaicin binds to prohibitin 2 and displaces it from the mitochondria to the nucleus. Biochemical and Biophysical Research Communications *379*, 519–525. https://doi.org/10.1016/j.bbrc.2008.12.103.

20. Janusz, J.M., Buckwalter, B.L., Young, P.A., LaHann, T.R., Farmer, R.W., Kasting, G.B., Loomans, M.E., Kerckaert, G.A., Maddin, C.S., and Berman, E.F. (1993). Vanilloids. 1. Analogs of capsaicin with antinociceptive and antiinflammatory activity. J Med Chem *36*, 2595–2604. https://doi.org/10.1021/jm00070a002.

21. Amantini, C., Mosca, M., Nabissi, M., Lucciarini, R., Caprodossi, S., Arcella, A., Giangaspero, F., and Santoni, G. (2007). Capsaicin-induced apoptosis of glioma cells is mediated by TRPV1 vanilloid receptor and requires p38 MAPK activation. J Neurochem *102*, 977–990. https://doi.org/10.1111/j.1471-4159.2007.04582.x.

22. Xu, S., Cheng, X., Wu, L., Zheng, J., Wang, X., Wu, J., Yu, H., Bao, J., and Zhang, L. (2020). Capsaicin induces mitochondrial dysfunction and apoptosis in anaplastic thyroid carcinoma cells *via* TRPV1-mediated mitochondrial calcium overload. Cellular Signalling *75*, 109733. https://doi.org/10.1016/j.cellsig.2020.109733.

23. Islam, A., Su, A.J., Zeng, Z.-M., Chueh, P.J., and Lin, M.-H. (2019). Capsaicin Targets tNOX (ENOX2) to Inhibit G1 Cyclin/CDK Complex, as Assessed by the Cellular Thermal Shift Assay (CETSA). Cells *8*, 1275. https://doi.org/10.3390/cells8101275.

24. Jia, G., Cang, S., Ma, P., and Song, Z. (2020). Capsaicin: A “hot” KDM1A/LSD1 inhibitor from peppers. Bioorg Chem *103*, 104161. https://doi.org/10.1016/j.bioorg.2020.104161.

25. Chen, H.Y., Lee, Y.H., Chen, H.Y., Yeh, C.A., Chueh, P.J., and Lin, Y.-M.J. (2016). Capsaicin Inhibited Aggressive Phenotypes through Downregulation of Tumor-Associated

NADH Oxidase (tNOX) by POU Domain Transcription Factor POU3F2. Molecules *21*, 733. https://doi.org/10.3390/molecules21060733.

26. Yang, F., Xiao, X., Cheng, W., Yang, W., Yu, P., Song, Z., Yarov-Yarovoy, V., and Zheng, J. (2015). Structural mechanism underlying capsaicin binding and activation of the TRPV1 ion channel. Nat Chem Biol *11*, 518–524. https://doi.org/10.1038/nchembio.1835.

27. Bertolin, G., Marchand, G.L., and Tramier, M. (2020). Real-Time Monitoring of Aurora kinase A Activation using Conformational FRET Biosensors in Live Cells. JoVE (Journal of Visualized Experiments), e61611. https://doi.org/10.3791/61611.

28. Goedhart, J. (2021). SuperPlotsOfData – a web app for the transparent display and quantitative comparison of continuous data from different conditions. MBoC, mbc.E20-09-0583. https://doi.org/10.1091/mbc.E20-09-0583.